Heliyon 9 (2023) e18221

Contents lists available at ScienceDirect

Heliyon

journal homepage: www.cell.com/heliyon

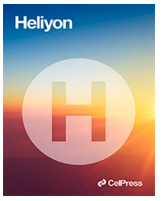

Novel glass-based membranes for Cu adsorption: From alkali activation to sintering

Diana Lago [a,*], Jozef Kraxner [a], Dušan Galusek [a,b], Enrico Bernardo [c]

[a] FunGlass – Centre for Functional and Surface Functionalized Glass, Alexander Dubček University of Trenčín, Študentská 2, 911 50, Trenčín, Slovakia
[b] Joint Glass Centre of the IIC SAS, TnUAD and FChFT STU, 911 50, Trenčín, Slovakia
[c] Department of Industrial Engineering, University of Padova, Via Marzolo 9, Padova, 35131, Italy

ARTICLE INFO

Keywords:
Porous membranes
Alkali activation
Cooper adsorption
Sintering

ABSTRACT

A porous membrane was developed through alkali activation of pharmaceutical boro-aluminosilicate glass powders suspended in diluted NaOH and KOH aqueous solutions (2.5 M). A consolidated porous structure was obtained by the binding of unreacted particles mediated by a surface gel, developed upon drying of the suspensions and their curing at 40 °C for 14 days. The binding phase was sufficiently stable to resist immersion in boiling water and in acidic solutions. Copper adsorption tests were carried out under acidic pH, immersing the membranes in a Cu $(NO_3)_2$ solution for different periods of time. To determine the effect of surface washing on capture of copper ions, adsorption experiments with washed and unwashed membranes were also carried out, at varying pH. It was determined that the adsorption kinetics follow the pseudo-second-order kinetic model. The main adsorption mechanism observed is the electrostatic interaction between the negative surface charge of the washed membrane and the Cu^{2+} ions present in solution. An adsorption higher than 60% was observed at pH = 5, while at pH = 2 the efficiency decreased due to the presence of H_3O^+ ions. To ensure immobilization of copper, the membranes were densified by viscous flow sintering at a moderate temperature (700 °C). Leaching tests on membranes demonstrated the efficiency of the process in terms of copper ions immobilization.

1. Introduction

In relation to other sectors, like agriculture and commerce, industry is one of the major consumers of water representing around 54% of the total water uptake in Europe, and 19% worldwide [1]. In terms of natural resources, water is at the center of sustainable development and is essential for socioeconomic growth, the preservation of healthy ecosystems and human survival [2]. The quality of water when turned into wastewater is markedly impaired due to the presence of inorganic ions, organic compounds, heavy metals, and other pollutants Briffa, 2020 [3]. According to the Environmental Protection Agency, the discharge of toxic metals, like copper, is limited to 1 ppm [4]. This implies the need for wastewater treatment before being discharged back into the environment.

In this context, global society needs approaches that minimize water consumption and focus on its recovery, following the principles of the circular economy Salviulo, 2021 [5]. In line with this, the development of technologies capable of treating wastewater

* Corresponding author.
E-mail address: diana.lago@tnuni.sk (D. Lago).

https://doi.org/10.1016/j.heliyon.2023.e18221
Received 2 April 2023; Received in revised form 11 July 2023; Accepted 12 July 2023
Available online 18 July 2023

should be considered. Immobilization of heavy metals using glass-based membranes shows a highly convincing alternative to solve this problem. The required materials (membranes) can be fabricated by a low-temperature consolidation process [6] of suitable alkali activated materials Luukkonen, 2019 [7].

The alkali activation concept is inherently bound to the research on geopolymers Provis J. L., 2014 [8]. According to Davidovits Davidovits, 2011 [9] geopolymers are the materials produced through the chemical reaction of an alumino-silicate material in an alkali hydroxide aqueous solution (alkali activation). The dissolution of the alumino-silicate promotes the release of hydrated alumino-silicate oligomers ("sialates"), followed by condensation reactions, leading to mostly amorphous gels with a characteristic three-dimensional network structure. Such network structure resembles that of crystalline zeolites ("zeolite-like gel"). In the network the SiO_4 and AlO_4 tetrahedra are connected via bridging oxygen atoms. The AlO_4 tetrahedra are stabilized by trapping the alkali ions in the network Provis J. L., 2014 [8].

The alkali activation yielding zeolite-like gels confers multiple advantages, such as low cost, fast hardening (even at room temperature), stability under chemical attack, high-temperature resistance, and a capability to immobilize and stabilize hazardous wastes Provis J. L., 2014 [10]. While glasses can trap a large variety of metal ions by their incorporation into the glass structure during the high temperature melting process (VG. [11]), geopolymers offer the same opportunity at a near room temperature, Lancellotti, 2010 [12].

Glasses play a multiform role in alkali activated materials. Soda-lime cullet may represent an 'activation aid' for the geopolymerization of relatively alumina-rich inorganic waste Toniolo, 2018 [13]: combined with alkali hydroxides, glass may provide additional alkali and silica, useful to tune the alkali-Al_2O_3–SiO_2 ratios, instead of a more expensive alkali silicate activator. Without alumina-rich waste, glass dissolves in alkaline solutions, but the reaction does not necessarily yield zeolite-like gels. For example, nearly Al_2O_3-free soda-lime glass is prone to formation of calcium silicate hydrates, [14], Rincón, 2017 [15].

Some alumino-silicate glasses are intentionally formulated to yield zeolite-like gels by alkali activation [16]. In the vast range of cullet, i.e., material recovered from the dismantling of a variety of glass articles, the (Ca-free) alkali boro-alumino-silicate glass (BASG) adopted for pharmaceutical containers (e.g., vials) has been recently found to offer unprecedented opportunities. The glass forms stable gels, even by the activation with diluted alkali hydroxide solutions, according to a mechanism proposed by Mehta et al. [6]. The activation results in the formation of a hydrated layer at the surface of fine glass particles; the particles are later bound to each other through condensation reactions. Alkali ions are involved only to a very limited extent in the gel that connects adjacent particles, since they form several hydrated carbonates, removed upon boiling.

Activated BASG from the pharmaceutical industry has been already tested for the adsorption of dyes: the new glass-based gels have been successfully tested in one of the emerging environmental applications of geopolymers, [6]. The present research aims at extending the applications of activated BASG in the remediation of wastewaters beyond organic pollutants; in particular, the immobilization of copper ions was considered. This was achieved through the physical and chemical bonding of the heavy metal ions in the solid matrix that reduced their mobility, minimizing the impact on the environment. After optimization of the pH, the activated BASG allowed for a first immobilization stage, achieved through adsorption of the heavy metal ions. A final stabilization was achieved by viscous flow sintering at 700 °C. The effectiveness of copper immobilization was evaluated by the measurement of the copper release from the matrix by leaching tests at 90 °C for 7 days.

2. Experimental methods

The boro-alumino-silicate glass cullet (BASG) from discarded clean pharmaceutical vials (production waste after quality check, from Nuova OMPI – Stevanato Group, Piombino Dese, Italy) was used as the starting material. Its chemical composition determined by X-ray fluorescence is shown in Table 1. Coarse glass fragments were crushed, milled in a planetary mill (Pulverisette 6, Fritsch GmbH), and sieved to obtain a powder with a particle size below 75 μm.

Fine powders were alkali-activated by immersion in NaOH/KOH 2.5 M aqueous solutions (50 mol%:50 mol%; Sigma Aldrich analytical grade), in a solid to liquid ratio of 60:40 (g/mL). The mixture was mechanically stirred (500 rpm) for 3 h at the room temperature to ensure the chemical reaction and dissolution of glass particles in the alkaline solution. Finally, the suspension was poured into an uncovered polystyrene container and cured at 40 °C for 14 days. After curing, a well-consolidated product was removed from the mold and cut into cubes of approximately 7 mm × 7 mm × 8 mm. A fraction of these was exposed to washing treatment in deionized water lasting 15 h, after which it was dried at 75 °C for 3 h. Washed and unwashed alkali-activated BASG samples were denoted as BASG-w and BASG, respectively. The dimensions of each cube were measured with a digital caliper. The surface area of each sample was calculated based on the measured dimensions and the geometric shape.

2.1. Adsorption experiments

At first, the effect of different experimental parameters on copper adsorption such as the membrane surface treatment (washing)

Table 1
Chemical composition of boro-alumino-silicate glass.

Chemical analysis (wt %)					
SiO_2	B_2O_3	Al_2O_3	Na_2O	K_2O	CaO
72 ± 2	12 ± 1	7 ± 0.3	6 ± 0.5	2 ± 0.1	1 ± 0.1

and pH of the solution, was studied. A stock aqueous solution of $Cu(NO_3)_2$ was prepared by dissolving analytical grade reagent (Sigma Aldrich) in deionized water. Then, it was diluted to obtain standard solution of 50 ppm of copper (pH 5). BASG and BASG-w cubes were put in contact with the copper solution. Subsequently, an aliquot of the solution was taken at different times to evaluate the adsorption kinetic. The adsorption tests were carried out at room temperature with mechanical agitation. The copper concentration in aqueous solution was determined by inductively coupled plasma-optical emission spectrometry (Spectro Genesis ICP-OES Analyzer Ametek), considering the difference between initial and final concentration. The copper removal efficiency and adsorption capacity (q (mg/g)) of the porous membranes were calculated by using equations (1) and (2), respectively.

$$\text{Efficiency} = \frac{(1 - C_e)}{C_0}\ 100, \tag{1}$$

and

$$q = \frac{C_0 - C_e}{m}\ V, \tag{2}$$

where C_0 is the initial concentration of copper in the solution (mg/L) and C_e the equilibrium concentration; V (L) is the volume of the solution, and m (g) is the mass of the membrane. The homogeneity of the copper adsorbed and its distribution within the membrane were examined by SEM/EDS. The same procedure was carried out with $Cu(NO_3)_2$ solution at pH 2 (after modification of pH of the original solution by adding HNO_3).

2.2. Surface charge density

The sorbent surface charge density is a fundamental parameter to determine the adsorption capacity of the studied material. The point of zero charge (pH_{PZC}) was determined on BASG and BASG-w samples by the pH drift method [17]. This procedure provides a quick yet reliable determination of pH_{PZC} Saha, 2020 [18]. For this measurement, the glass was milled, and the powder (<75 μm) was put in contact with deionized water which was previously acidified/alkalinized with HCl/NaOH. The pH of the solutions was adjusted to pH values between 1 and 11. For each solution, 0.5 g of glass powder was added, and the suspension was kept closed with mechanical stirring for 15 min before measuring the pH value. The pH_{PZC} is the point where $pH_{initial}$ and pH_{final} values are equal [17].

2.3. Sintering

Sintering experiments were performed after copper adsorption on BASG and BASG-w samples from room temperature up to 700 °C in air, using a heating rate of 5 °C/min and 1 h isothermal dwell at the maximum temperature.

2.4. Leaching experiments

To evaluate the aqueous corrosion resistance, leaching tests were performed on sintered samples following the Materials Characterization Center-1 procedure (MCC-1: ASTM C1220-10). The samples were placed in Teflon containers with deionized water at a sample surface area to water volume ratio (S/V) of 10 m^{-1}, in line with the reference matrix A. The reference matrix A is a reference test used to measure the effects of waste loading, e.g., on the chemical durability of the waste form. The leaching experiments were carried out at 90 °C in static regime; an aliquot of the leachate was taken after 7 days and chemically analyzed by ICP-OES. At the end of the leaching test, the samples were removed from the solution, dried at 75 °C for 3 h and weighed. With the weight loss measurements, the gravimetric dissolution rate GDR (g/m^2d) was calculated using equation (3):

$$GDR = \frac{\Delta m}{st} \tag{3}$$

where Δm is the weight loss (g), s is the initial geometric area of the sample (m^2), and t is the leaching time (days).

The chemical stability and physical integrity of the BASG was analyzed placing some cubes in falcon tubes with acid media (HNO_3–HCl, pH 1) with a solid to liquid ratio of 20 g/L for 30 days. After that, the samples were dried their surface chemically analyzed.

2.5. Samples characterization

The samples obtained after different treatments were characterized in terms of their chemical composition and microstructure using energy dispersive spectroscopy (EDS/EDAX Genesis), scanning electron microscopy (FEI, Quanta 200 ESEM) and Fourier transform infrared spectroscopy (FTIR Jasco 4200). In the FTIR measurements, the spectra were recorded between 4000 and 400 cm^{-1}. X-ray diffraction analyses were carried out on powder samples using a diffractometer (XRD Brucker D8 Advance) operating at 40 kV and 40 mA with CuKα radiation (0.15418 nm) between 9 and 70° of 2θ, with a step size of 0.02° and counting time of 2 s per step. The phase identification was performed with the software HighScore Plus v. 3.0d, (PANanalytical B.V. 2011).

The bulk density of the alkali-activated and sintered samples was measured geometrically considering the mass measured with an analytical balance and the volume of the samples measured with a digital caliper. Helium pycnometry (Ultrapyc 3000, Anton Paar

GmbH) was used to determine the apparent and true density of the samples. The porosity of the samples was calculated with the values obtained by these measurements. Each data point represents an average value of 4–6 individual tests.

3. Results and discussion

Table 2 shows the chemical composition of BASG and BASG-w samples, respectively. The results document that the washing treatment removed the excess of alkali.

Fig. 1 shows the SEM micrographs of the cross sections of alkali-activated BASG after 14 days of curing at 40 °C before (a-b) and after (c-d) washing treatment. The elemental maps in Fig. 1b and (d) give details about the chemical distribution of the elements present in Fig. 1a and (c), respectively.

Before washing (Fig. 1a) the glass particles appeared to be 'glued' together, but some areas coincided with higher concentrations of sodium and potassium, as documented by the element mapping (Fig. 1b). In particular, some gel effectively covered the glass surfaces (Fig. 1a), but the spaces between adjacent particles contained alkali-rich crystals. After washing, the morphology of the sample was more homogeneous (Fig. 1c), with no chemical gradient between individual particles (Fig. 1d). As a consequence, an abundant open porosity originated from the incomplete packing of glass particles.

As observed previously, alkaline attack of BASG yields quite specific results [6]. Unlike in Ca-rich and Al-poor common soda-lime glass, alkali activation does not promote formation of calcium silicate hydrated (CSH) compounds. On the contrary, the dissolution of BASG dissolves the components (silicates, borates and aluminates) which may be responsible for the development of stable zeolite-like gels. The stability of the formed gels was confirmed by the resistance of the dried and cured compacts to boiling water.

The results of FTIR and XRD analysis (Fig. 2) confirmed the development of a 'mixed' binding phase between unreacted particles. OH^- ions disrupted the glass network, breaking the oxygen bridges. The related dissolution products, along with alkaline ions from the solution, which were originally bound in the boro-alumino-silicate network to stabilize BO_4 and AlO_4 units, interacted with each other and with the atmosphere, forming multiple phases.

Fig. 2a shows the FTIR spectra of dried and cured samples. The Si–O stretching (at 1000-1030 cm^{-1}) and Si–O–Si bending vibration (around 800 cm^{-1}) characteristic of the glass matrix Aguiar, 2009 [19], remain well visible, but with important modifications, depending on the conditions of treatment (as-received, activated, washed). The signals of the as-received and washed material are similar, whereas the alkali activation process caused a shift of the main peak from 1020 cm^{-1} to 979 cm^{-1}. The shift was attributed to the replacement of SiO_4 units with AlO_4 upon gelation, Longhi, 2019 [20]. This effect is also observed in the displacement and reduction of the intensity of the Si–O–Si bending peak around 800 cm^{-1} after alkali activation, indicating the formation of hydrated gel after the activation.

In our opinion, the condensation of Si–OH, Al–OH and B–OH terminations led to reconstruction of the oxygen bridges in the original glass structure, with permanent bonding of adjacent particles. Some components, after dissolution and condensation yielded an additional alkali-richer boro-alumino-silicate phase in the interstices between adjacent particles, as documented by the shifts of the main FTIR peaks. The alkali enrichment could cause a severe network depolymerization, promoting solubilization upon washing. After alkali activation, the peaks observed in the FTIR spectra (solid red) at 594 cm^{-1}, 690-700 cm^{-1}, and 1600 cm^{-1} are consistent with the results of Garcia Lodeiro et al. related to the formation of N-A-S-H gels in the presence of alkalis, García-Lodeiro, 2008 [21].

Alkalis could react also with atmospheric CO_2 (M. [22]). The C–O stretching signal at around 1410 cm^{-1} (asymmetric stretching vibration), detected after activation but not after washing, is consistent with the formation of soluble (hydrated) carbonates.

The mineralogic analysis (Fig. 2b) provided additional information: the newly formed material after activation was semi-crystalline. The as-received glass exhibited only the typical halo of amorphous materials at $2\theta = 15–40°$. After washing, the pattern was nearly identical to that of the as-received glass. On the contrary, the diffractogram of the alkali-activated glass featured important contributions from newly formed phases. Most reflections corresponded to hydrated sodium silicate hydroxide ($NaSi_4O_8(OH)\cdot 4H_2O$, # 48–0655) and hydrated sodium carbonate ($Na_2CO_3\cdot H_2O$, #76–0910). The relatively high solubility of the last one (215 g/L at 20 °C) [23], explains the absence of its characteristic reflections in the diffractogram obtained after washing of the BASG. The reflections at $2\theta = 30$ and 37.9° could possibly correspond to $KAlSi_3O_8\cdot H_2O$ (#16–0385).

Washing resulted in a kind of 'etching' of the soluble (both amorphous and crystalline) newly formed phases, as confirmed by the results of density measurements reported in Table 3. The pycnometry analysis confirmed the removal of material in the contacts between packed particles, documented by the parallel increase of both overall and open porosity (from 33 to 39% and from 30 to 37%, respectively). The increase of open porosity represents an advantage in terms of capturing additional material, as will be discussed later for adsorption of copper.

Regarding the compressive strength of BASG, it was measured in a previous work determining a value of 19.8 ± 1.5 MPa Tameni, 2022 [24]. By combining the measured density value with this compressive strength, makes membranes comparable to commercial

Table 2
Chemical composition of alkali-activated BASG before and after washing.

Sample	Chemical analysis (wt %)						
	C	O	Na	Al	Si	K	Ca
BASG	10.5 ± 0.9	50 ± 5	14 ± 3	2.1 ± 0.07	18.5 ± 2	4 ± 0.3	0.8 ± 0.05
BASG-w	–	51.2 ± 6	6 ± 0.6	4 ± 0.3	36 ± 3	1.5 ± 0.06	1.2 ± 0.04

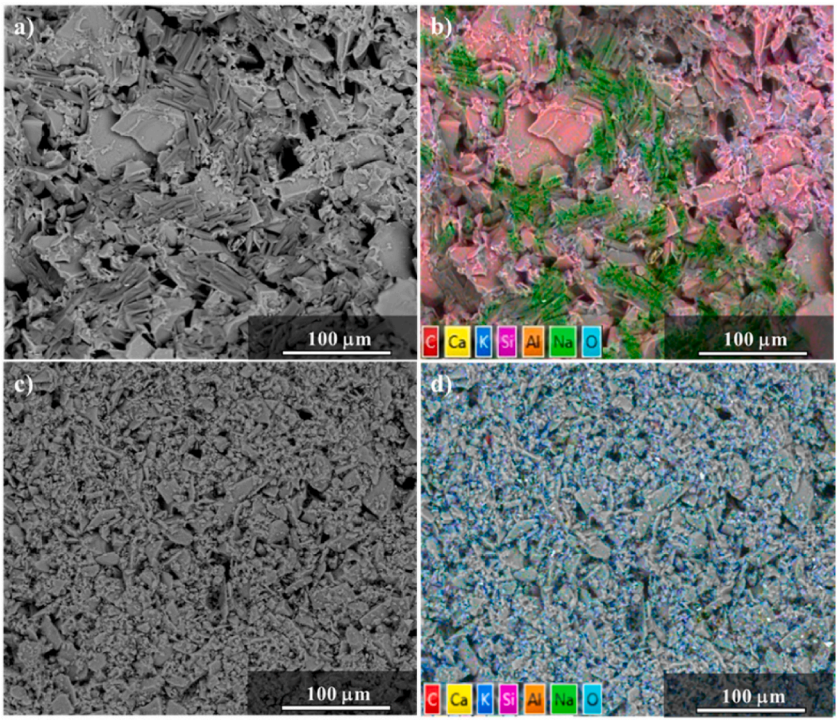

Fig. 1. SEM micrographs of the alkali-activated glass: a-b) before and c-d) after washing. Fig. 1(b) and (d) show the element maps of the regions in Fig. 1(a) and (c), respectively.

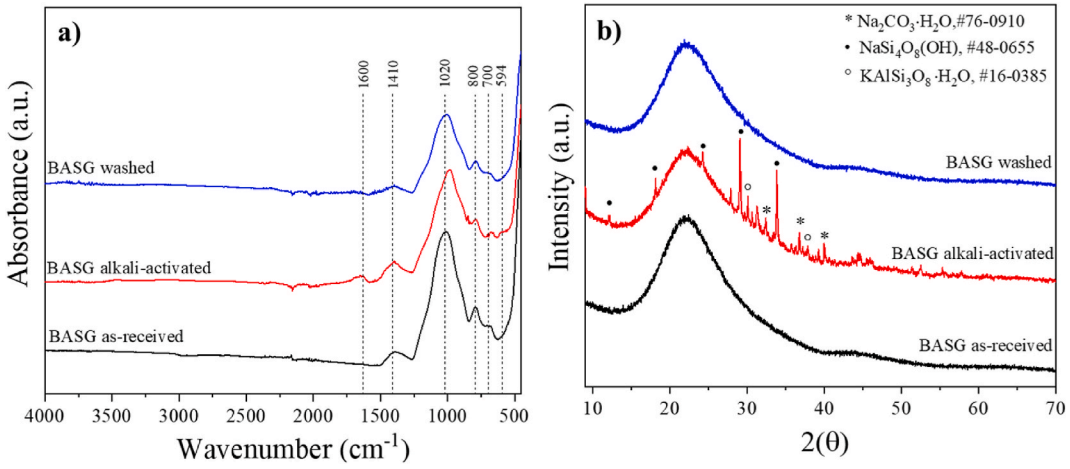

Fig. 2. a) FTIR spectra and b) X-ray diffraction patterns of the as-received BASG, alkali-activated and washed. The wavenumbers shown in the FTIR spectra correspond to the peaks of the as-received BASG.

Table 3
Density and porosity of BASG and BASG-w samples before and after washing.

Sample	Density, ρ (g/cm^3)			Porosity (%)		
	Geometric	Apparent	True	Total	Open	Closed
BASG	1.63 ± 0.23	2.31 ± 0.05	2.42 ± 0.19	33 ± 2	30 ± 2	3 ± 2
BASG-w	1.51 ± 0.13	2.39 ± 0.23	2.45 ± 0.16	39 ± 2	37 ± 2	2 ± 1

construction materials, such as lightweight concrete.

One of the well-known methods for the treatment of wastewater is filtration of contaminated solutions. Different treatment procedures were developed and applied. Metal ions can be removed from the solution by adsorption, but also by capillary forces related to the porosity of the sample [25]. Such treatment is highly dependent on the experimental parameters of the assay, as well as the material's characteristics. The adsorption capacity of a sorbent is influenced by the synthesis method, which determines, among others, the surface charge density, specific surface area, and porosity of synthesized material Rouquerol, 2013 [26].

On the other hand, the pH of the solution is an important factor which determines the speciation of the surface functional groups of the adsorbate in the solution and the degree of ionization and ions speciation, Mihaly-Cozmuta, 2014 [27]

Fig. 3a shows the results of the measurement of the pH_{PZC} for BASG and BASG-w samples using the pH drift method. The pH_{PZC} is the pH value where negative ($[MO^-]$) and positive ($[MOH_2^+]$) surface concentrations are equal, Gulicovski, 2008 [28]. The pH_{PZC} is the value at which the initial and the final pH are the same.

The pH_{PZC} value determined for BASG-w and BASG was almost identical (1.5–2). When the pH value of the solution is higher than pH_{PZC}, the glass becomes deprotonated and exhibits negative surface charge (and positive at $pH < pH_{PZC}$).

These values agree with previous studies showing that borosilicate glasses and silica surfaces in acidic solutions are negatively charged [29]. The present results are explained considering that aluminium and boron may be four-fold coordinated with respect to oxygen; the negative charge imbalance can only be compensated by the presence of alkaline ions or cations (e.g., Cu^{2+} coming from the heavy metal solution as it will be shown later). The surface washing treatment removes the excess of alkaline ions, keeping the stability of the formed gel and preserving the inherent negative charge. This implies the possibility that copper ions are bound to the membrane surface through adsorption. Depending on the pH of the aqueous media, Cu^{2+} ions could compete with H_3O^+ ions for the surface-active sites influencing the amount of copper that can be adsorbed.

Fig. 3b shows the copper adsorption capacity (left panel) and efficiency (right panel) of BASG-w as a function of time for the solutions at pH 5 and 2. The measurements were carried out analyzing the adsorption of copper ions from the solution (50 ppm Cu) with the pH (5), and after modifying it to pH (2) by HNO_3 addition. Depending on the pH of the medium, the behaviour was completely different. The adsorption increases when carried out in a pH 5 solution, while it is almost null in the acidified solution ($1 \pm 0.7\%$).

In the solution with pH 5, the adsorption rate is high during the first hours because of the large number of negatively charged sites in BASG-w available for the adsorption. As Cu^{2+} ions bind to those sites, their availability is reduced and the adsorption rate decreases, remaining stable until an equilibrium is reached. At the end of the experiment, the adsorption efficiency reached $62 \pm 3\%$. It is worth mentioning that other publications in which equivalent copper adsorption efficiencies have been obtained (60–80%), under similar experimental conditions, refer to activation of the starting material by more concentrated alkaline solutions (Na_2SiO_3 5M − NaOH 10 M) Šuránek, 2023, Baykara, 2022 [30–32]. In addition, the curing time used in the synthesis of the porous materials was at least 20 °C higher than the temperature used in this work (40 °C). This reflects less stringent synthesis conditions and the great versatility of the BASG used in our work to prepare porous membranes.

At the low pH value (2) the lower adsorption is related to the higher concentration of H_3O^+ ions which compete with the Cu^{2+} ions for the negatively charged sites on the surface. The preferential adsorption favours H_3O^+ over Cu^{2+} ions. As the solution pH value increases, the electrostatic repulsion between the negatively charged sites on the surface of BASG-w and cations decreases, adding to the fact that fewer H_3O^+ ions are available to compete with Cu^{2+} ions for the active sites [33].

It should be noted that the formation of a precipitate was observed during the adsorption test with the unwashed sample (BASG). In other words, copper ions were incorporated into the soluble material placed in the voids between particles discussed above. Although a certain degree of adsorption was achieved and demonstrated by the change of color in the sample, the values obtained by ICP-OES were erratic. This was attributed to the fact that the concentration of copper ions available in the solution decreased due to the formation of precipitates, and the results of chemical analysis do not reflect the actual extent of adsorption. If the effect of washing is considered, the

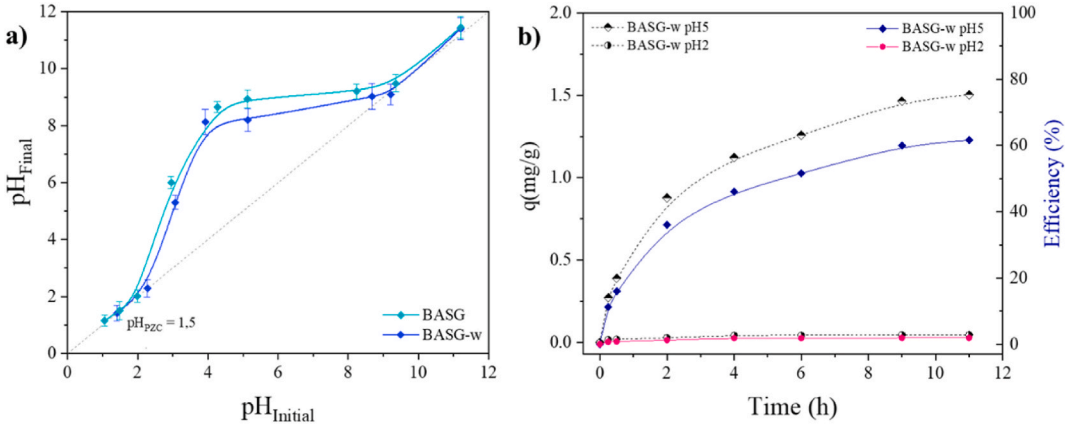

Fig. 3. a) pH_{PZC} measurement on BASG and BASG-w samples, using the pH drift method, and b) adsorption capacity (left panel) and efficiency (right panel) of BASG-w sample as a function of time in $Cu(NO_3)_2$ at pH 5 and 2. The lines serve as a guide to the eyes.

decrease of the adsorption capacity of the BASG (unwashed) sample can also be attributed to the excess of alkalis present on the surface of the material.

The pH of the solutions was registered before and after the adsorption tests, observing a significant increase in the pH values of the solution for BASG (from pH 5 to 10), compared with only a negligible pH increase in BASG-w (from pH 5 to 5.3). This increase in the pH value was related to an increase in the concentration of hydroxyl ions in the solution, when the BASG sample was in contact with the Cu $(NO_3)_2$ solution. The process can be schematically described by the following reaction equations:

$$BASG_{(s)} + NaOH_{(ac)} : K(OH)_{(ac)} \rightarrow BASG\{Na, K(OH)\}_{(s)} \text{ or directly BASG}$$

$$BASG_{(s)} + Cu(NO_3)_{2(ac)} \rightarrow BASG_{(s)} + \mathbf{Cu^{+2}_{(ac)}} + (NO_3)^{-2}_{(ac)} + Na^{+}_{(ac)} + K^{+}_{(ac)} + \mathbf{OH^{-}_{(ac)}} \uparrow \mathbf{pH}$$

From the speciation diagram Demirbas, 2009 [34], it is inferred that Cu^{2+} ions represent a dominant copper species at the pH values lower than 6. However, the formation of copper hydroxides takes place from pH 6. The reaction between the hydroxyl groups released from BASG and copper solution leads to the formation of $Cu(OH)_2$, an extremely insoluble compound ($Ksp = 1.6 \times 10^{-19}$ at 25 °C), [23]. The presence of a precipitate was confirmed during the adsorption test with the BASG sample. The precipitated product was analyzed by FTIR. Fig. 4 shows the spectra for the precipitate that was collected and dried at low temperature (75 °C for 3 h) from the bottom of the vessel after the adsorption test. The spectra of the glass after activation and adsorption were also added for comparison.

The FTIR spectrum of the precipitate presents a strong peak at 3536 cm^{-1} corresponding to free O–H group and a broad peak at 3391 cm^{-1} related to hydrogen bonded O–H groups Devamani, 2013 [35]. Another smaller peak at 1670 cm^{-1} corresponds to the bending mode of the hydroxyl group of water. The infrared spectrum of the precipitate is characterized by intense bands centered around 1420 and 1318 cm^{-1} which are attributed to the $(CO_3)^{2-}$ stretching modes. These results are consistent with those published by [36] related to the mineral $Cu_2CO_3(OH)_2$. The peak at 881 cm^{-1}, present in the sample after adsorption, indicates Cu–OH vibrations Henrist, 2003 [37].

The bands at 874, 770, and 676 cm^{-1} were found in good agreement with Aguirre et al. work (876, 781, and 676 cm^{-1}) corresponding to Cu–OH bonds, [38].

The copper adsorption kinetics was also analyzed using the pseudo-first-order (PFO) and pseudo-second-order (PSO) models. The PFO model may show properties of Langmuir rate equation at initial times of adsorption or close to equilibrium. In these conditions, the change of adsorbate concentration in solution or change in the relative surface coverage during the adsorption process is small. Another kinetic model extensively used is the PSO which assumes that the rate limiting step is the chemical adsorption, Azizian, 2004 [39]. The corresponding expressions are given by equations (4) and (5), respectively.

$$\ln(q_e - q_t) = \ln q_e - kt \tag{4}$$

$$\frac{t}{q_t} = \frac{1}{kq_e^2} + \frac{1}{q_e}t \tag{5}$$

where q_e and q_t (mg/g) are the copper adsorption capacity at an equilibrium and at time t respectively, and k (min^{-1}) is the rate

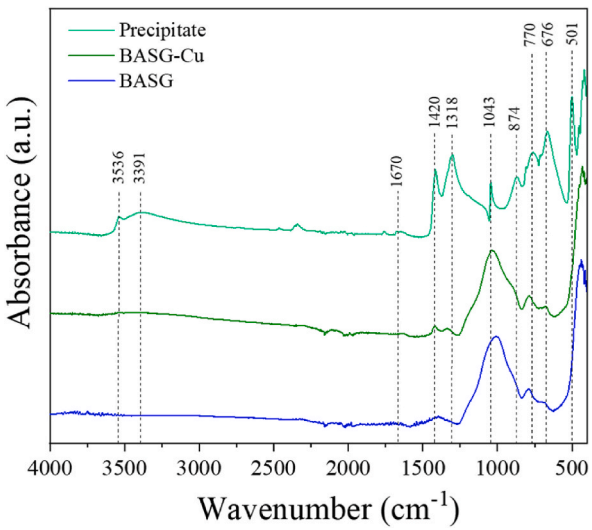

Fig. 4. FTIR spectra of the alkali-activated borosilicate glass (solid blue), after copper adsorption (solid green) and the precipitate (solid bright green). The wavenumbers shown in the FTIR spectra correspond to the peaks of the precipitate obtained after the adsorption test with the BASG. (For interpretation of the references to color in this figure legend, the reader is referred to the Web version of this article.)

constant. Fig. 5 shows the fitting of the experimental data. The PFO and PSO plots for copper adsorption on BASG-w membranes at pH 2 and 5 are respectively shown in Fig. 5 a, c and Fig. 5 b, d.

The results of the fitting show good agreement of the experimental data with the kinetic models. The obtained kinetic parameters are presented in Table 4. The correlation coefficients for the PSO model were higher ($R^2 = 0.9947$ and 0.9922) than for the PFO model ($R^2 = 0.9168$ and 0.9677) for the data measured at pH 2 and 5, respectively. However, it is necessary to point out that the lower value of the correlation coefficient of the acidic solution (pH 2) is related to the low adsorption value.

The highest correlation coefficient obtained by fitting the experimental data with the PSO kinetic model indicated that the adsorption process took place via several mechanisms, including chemical interaction and electrostatic attraction of copper ions with binding sites on the surface of membranes.

It was observed that the copper adsorption process on BASG-w membranes is kinetically viable. Since adsorption is a thermally activated process, its thermodynamic feasibility will be evaluated in future studies.

Adding to the fact that BASG-w exhibited better copper adsorption than the unwashed sample, it can be also concluded that the cold consolidation process yielded the bodies capable of resisting very strong acidic conditions without disintegration.

Chemical analysis of the alkali-activated borosilicate glass immersed in acid solution (pH 1) for 30 days revealed chemical composition very close to the nominal composition of the original glass (49.9% O, 7.4% Na, 4% Al, 36% Si, 1,2% K, 1.4% Ca (wt%)). This fact confirms stability of the formed material, even at pH values as low as 1. Such unwashed membrane could be thus used to handle also highly acidic wastewaters.

As a part of the approach proposed to immobilize copper in porous membranes obtained by alkali activation of a boro-aluminosilicate glass, both samples (BASG and BASG-w) were subjected to non-isothermal sintering treatment. The aim of the process was to identify the minimum temperature required to maximize densification. A low temperature reduces partial vapor pressures, minimizing potential evaporation of volatile compounds, like copper nitrate, during heavy metal immobilization, [40].

The prepared blocks were densified at a relatively low temperature, above the glass transition temperature of the boro-aluminosilicate, T_g 550 °C, Rincón, 2017 [15]. The importance of knowing the T_g value lies in the fact that both the crystallization and viscous flow sintering kinetics are appreciable only at temperatures higher than T_g, [41]. Therefore, the T_g represents a lower limit for sintering.

Ray et al. reported that the optimum sintering temperature could be estimated 50 °C above the dilatometric softening temperature (A. [42]). In our previous works the dilatometric sintering temperature of BASG was determined to be about 650 °C (Bernardo E. &., 2004) [43]. In this work, the sintering was carried out at 700 °C for 1 h at the heating rate of 5 °C/min. Fig. 6 shows the EDS elemental maps of the alkali-activated glass and microstructural details of both samples after adsorption tests and after sintering. The chemical composition of each sample is also included.

After adsorption, the surface of the BASG-w sample was covered by a layer of small, homogeneously distributed copper aggregates (Fig. 6a). This was reflected in the content of copper on the glass surface (16.5%) and also in its distribution on the compositional map. On the surface of the unwashed sample (Fig. 6c) the presence of copper is visibly lower: copper appears in the form of discreet particles

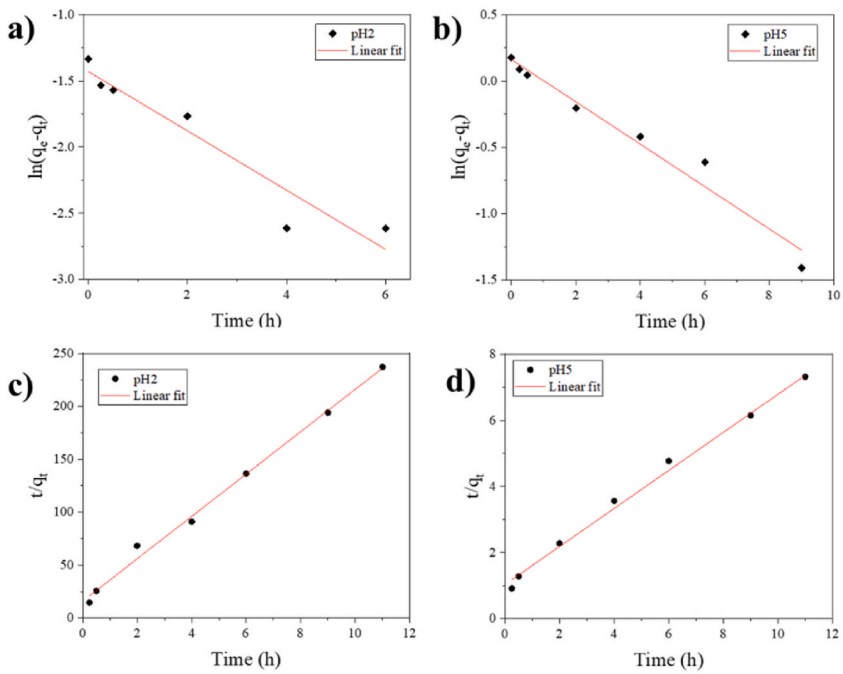

Fig. 5. Kinetic model plots for copper adsorption on BASG-w membranes: (a, b) pseudo-first-order, and (c, d) pseudo-second-order models. Fig. 5(a) and (c) show adsorption data at pH 2, while (b) and (d) depict adsorption data at pH 5.

Table 4
Pseudo-first-order (PFO), and pseudo-second-order (PSO) model and correlation coefficients for copper adsorption on porous BASG-w membranes.

Model	PFO (Eq 4)		PSO (Eq 5)	
	k	R2	k	R^2
BASG-w, pH 2	−0.2239	0.9168	19.8657	0.9947
BASG-w, pH 5	−0.1598	0.9677	0.5750	0.9922

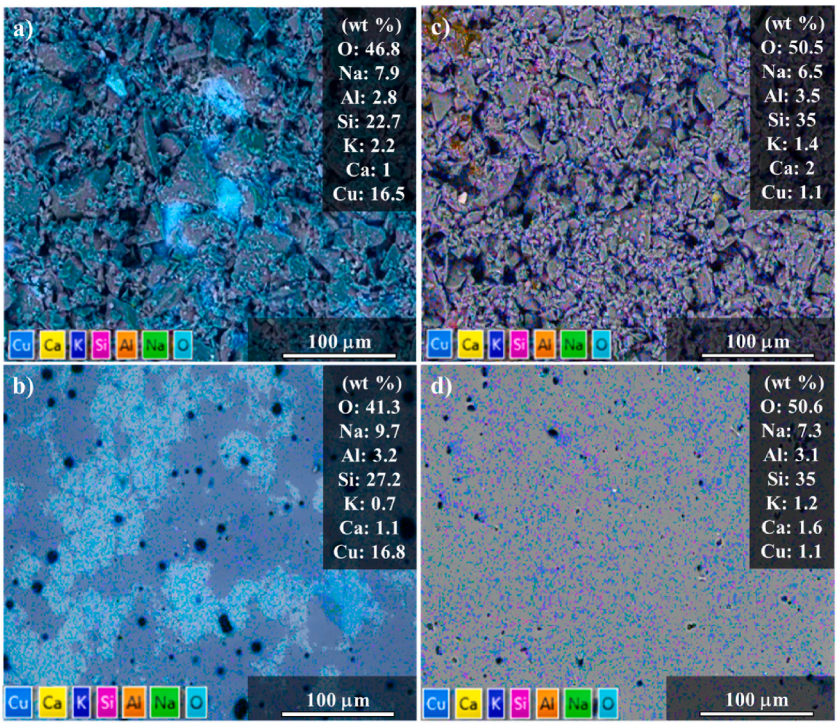

Fig. 6. EDS elemental maps of the alkali-activated glass: (a–b) BASG-w and (c–d) BASG. Fig. 6(a) and (c) show the samples after adsorption, while (b) and (d) depict the microstructure and final porosity of the samples after sintering.

dispersed on the surface of the sample. The map does not record areas with a higher concentration of copper, due to the lower overall amount of adsorbed copper (1%) and a homogeneous distribution of the mapped elements.

After sintering at 700 °C the BASG and BASG-w samples appear well densified (Fig. 6b and d). In particular, copper present in the BASG-w sample after adsorption (Fig. 6b) is present as large aggregates of massive habit, but also in the matrix. After sintering, it is present on the glass surface almost in the same proportion as after adsorption (16.8%). Likewise, the content of copper in the BASG sample (1%) is the same both before and after sintering (Fig. 6d).

Structural consolidation was achieved in both samples, as a result yielding compact bodies with smooth surfaces (Fig. 6d). This is also reflected in the shrinkage of 6 ± 2% for BASG-w (compared to 2 ± 0.5% for BASG), causing a decrease in the overall porosity.

Table 5 shows that although the overall porosity was reduced after sintering, some pores remain visible. The result is a combination of an increase in the amount of closed porosity, probably due to the presence of trapped gases during sintering, and a decrease in the amount of the open porosity. The open porosity decreased in comparison to that obtained after alkaline activation (24 and 29% for the BASG and BASG-w samples, respectively). This implies a lower probability of the interaction between the water from the leaching media and the interior of the membrane with the consequent decrease of the leaching rate.

Sintering also led to stabilization of the copper adsorbed on alkali-activated BASG, as was observed in the chemical analyses

Table 5
Density and porosity of BASG and BASG-w samples after sintering.

Sample	Density, ρ (g/cm^3)			Porosity (%)		
	Geometric	Apparent	True	Total	Open	Closed
BASG,700	1.56 ± 0.18	1.65 ± 0.16	1.97 ± 0.21	21 ± 2	6 ± 2	15 ± 3
BASG-w, 700	1.54 ± 0.12	1.67 ± 0.05	2.25 ± 0.25	32 ± 3	8 ± 1	24 ± 2

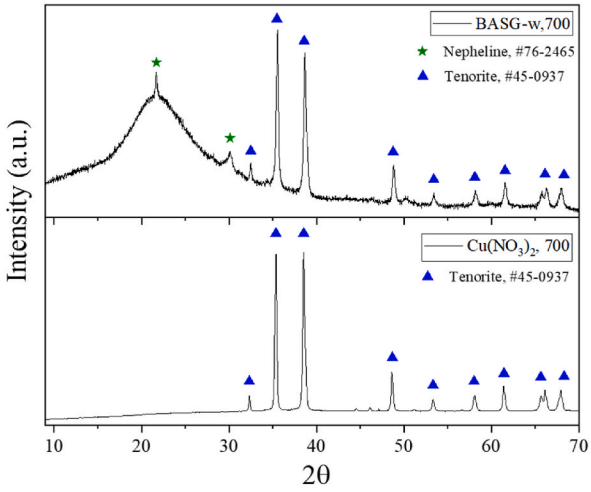

Fig. 7. X-ray diffraction of BASG-w after sintering (top panel) and the product obtained after subjecting $Cu(NO_3)_2$ powder to the same heat treatment (bottom panel).

performed before and after sintering. A change in the coloration of the samples was observed after sintering in air (from light blue to black), possibly due to the formation of copper oxide. The presence of copper oxide was also corroborated by X-ray diffraction analysis. Fig. 7 shows the diffractograms of BASG-w after sintering (top panel) and copper nitrate subjected to the same heat treatment, 700 °C-1h, (bottom panel): the main lines correspond to tenorite (cupric oxide, CuO, #45–0937). Weak signals in the diffractogram of the sintered BASG-w (bottom panel) are attributed to nepheline (sodium and potassium alumino-silicate, $Na_3KAl_4Si_4O_{16}$, #76–2465). Cupric oxide presence agrees with the work of Morozov et al. according to which the oxide known as tenorite can be obtained by heat treatment of $Cu(NO_3)_2$, $Cu(OH)_2$, $CuCO_3$ at 200–250 °C Morozov, 2003 [44].

The main parameter that defines the efficiency of heavy metal immobilization process is the resistance of the products obtained from sintering to aqueous corrosion. Leaching tests were carried out by placing sintered samples in distilled water at 90 °C for 7 days, following the MCC-1 procedure. The final appearance of sintered samples after the leaching tests was that of well-consolidated compacts that did not show any disintegration or crack formation. Gravimetric dissolution rates were determined after drying and weighing the samples subjected to the leaching tests. The values obtained, $6{\cdot}10^{-2}$ and $8{\cdot}10^{-2}$ g/m^2d for BASG-w and BASG, respectively, were comparable or better to those of other glasses used in the immobilization of heavy metals by sintering, [45].

Chemical analyses of the leaching solutions showed the copper concentrations of $3{\cdot}10^{-2}$ and below $1{\cdot}10^{-4}$ ppm for BASG-w and BASG, respectively. The low value obtained for the BASG sample corresponds with the lowest amount of the adsorbed copper. For the BASG-w sample, which adsorbed more than 60% of copper from the solution, the leached copper concentration in the solution was more than two orders of magnitude lower than the EPA limit value for copper (1 ppm) [4]. This suggests compliance with the requirements established for the disposal of inert and non-hazardous waste in sanitary landfills, [46].

The glass constituent elements (Si, B, Al, Na, K, Ca) were also analyzed, obtaining in all cases concentrations below the detection limit of the technique. This demonstrates that copper stabilization benefits from the high chemical durability of pharmaceutical glass.

As a final remark, the development of materials with new features from the recycling of discarded materials is essential to reduce the environmental impact caused, for example, during the production of cement (and even the exploitation of the minerals required for its manufacture). To evaluate the economic feasibility of the proposed process, it is necessary to consider one of the most important contributions, which is the one referring to transport. The impact of this variable in our case is minimized with the use of glass cullet from the Italian pharmaceutical industry, reducing the transportation costs of the raw material. Even depending on the chemical formulations of the discarded cullet, products comparable to bricks were obtained directly after firing the alkali-activated glass at low temperature Tameni, 2022 [24]. Added to this, the use of a lower sintering temperature (700 °C) than those required for glass melting (>1000 °C), implies less energy consumption (and wear on associated equipment, furnaces, specifically).

From an environmental point of view, it is necessary to emphasize that CO_2 emission in alkali-activated materials is mainly during production of activators (alkali hydroxide and silicate from carbonates) [47]. The use of low molarity alkaline solutions (NaOH, KOH 2.5 M) in our work implies less environmental impact when managing associated waste, as well as the process associated with its production. Finally, some authors of this work even observed that in the preparation of alkaline solutions industrial sludge could be used instead of water, favoring the reduction of the use of drinking water Tameni, 2022 [24].

4. Conclusions

Discarded pharmaceutical glass cullet was chemically treated for the fabrication of sorbent membranes capable of the uptake of copper from aqueous solutions. The alkali activation and sintering of the boro-alumino-silicate glass represented the best compromise between low processing temperature, chemical durability, and immobilization of heavy metal ions. The main mechanism observed for

copper adsorption is the electrostatic interaction resulting from the negative surface charge of the washed membrane and the Cu^{2+} ions at pH value of 5. For extremely low pH values (2) a decrease in adsorption is observed because of the competition between Cu^{2+} and H_3O^+ ions present in the medium. The kinetic models used in the fitting of the adsorption data indicated that copper adsorption was faster in the first moments of the adsorption test: the BASG-w membrane surface was covered with the adsorbate due to the high initial copper concentration and hence, its better availability. This was reflected in the higher values of the correlation coefficient of PSO model ($R^2 = 0.9922$ and 0.9947) in relation to the PPO model ($R^2 = 0.9677$ and 0.9168), for adsorption at pH 5 and 2, respectively.

However, unwashed membranes are also suitable for the treatment of acidic solutions. The chemical analysis confirmed their high stability during their immersion in an acidic solution for 1 month.

Sintering at a relatively mild conditions (700 °C-1h) efficiently immobilized the adsorbed copper, minimizing losses due to volatilization. Short leaching tests (7 days) confirmed the chemical durability of the product and its ability to immobilize copper.

Author contribution statement

Diana Lago: Conceived and designed the experiments; Performed the experiments; Analyzed and interpreted the data; Wrote the paper.

Jozef Kraxner: Contributed reagents, materials, analysis tools or data.

Dušan Galusek: Contributed reagents, materials, analysis tools or data; Wrote the paper.

Enrico Bernardo: Conceived and designed the experiments; Analyzed and interpreted the data; Contributed reagents, materials, analysis tools or data; Wrote the paper.

Data availability statement

Data will be made available on request.

Declaration of competing interest

The authors declare that they have no known competing financial interests or personal relationships that could have appeared to influence the work reported in this paper

Acknowledgements

This paper is a part of the dissemination activities of the FunGlass project. This project has received funding from the European Union's Horizon 2020 research and innovation programme under grant agreement No. 739566. The authors also gratefully acknowledge the financial support from the Slovak Grant Agency of the Ministry of Education, Science, Research and Sport, VEGA No 1/0456/20. Publication was created also in the frame of project: Advancement and support of R&D for Centre for diagnostics and quality testing of materials in the domains of the RIS3 SK specialization, ITMS2014+:313011W442, based on the Operational Programme Integrated Infrastructure and funded from the European Regional Development Fund.

References

[1] FAO, AQUASTAT Main Database', Food and Agriculture Organization of the United Nations, 2016. Retrieved from, http://www.fao.org/nr/water/aquastat/data/query/index.html?lang=en.
[2] Water U.N.. 2018 UN world water development report, Nature-based Solutions for Water, 2018.
[3] J.S. Briffa, Heavy metal pollution in the environment and their toxicological effects on humans, Heliyon 6 (9) (2020), e04691.
[4] S. Biswas, Treatment of copper contaminated municipal wastewater by using UASB reactor and sand-chemically carbonized rubber wood sawdust column, BioMed Res. Int. 2016 (9) (2016).
[5] G.L. Salviulo, Enabling circular economy: the overlooked role of inorganic materials chemistry, Chem.–Eur. J. 27 (22) (2021) 6676–6695.
[6] A.K. Mehta, Upcycling of pharmaceutical glass into highly porous ceramics: from foams to membranes, Materials 15 (11) (2022) 3784.
[7] T.H. Luukkonen, Application of alkali-activated materials for water and wastewater treatment: a review, Rev. Environ. Sci. Biotechnol. 18 (2) (2019) 271–297.
[8] J.L. Provis, Geopolymers and other alkali activated materials: why, how, and what? Mater. Struct. 47 (1) (2014) 11–25.
[9] J. Davidovits, Geopolymer Chemistry and Applications, third ed., Geopolymer Institute, 2011.
[10] J.L. Provis, Geopolymers and related alkali-activated materials, Annu. Rev. Mater. Res. 44 (2014) 299–327.
[11] V.G. Scarinci, G. B, Glass foams, in: P.C.M. Scheffler (Ed.), Cellular Ceramics: Structure, Manufacturing, Properties and Applications, KGaA, Weinheim: WILEY-VCH Verlag GmbH & Co, 2005, pp. 158–176.
[12] I.K. Lancellotti, Chemical stability of geopolymers containing municipal solid waste incinerator fly ash, Waste Manag. 30 (4) (2010) 673–679.
[13] N.R. Toniolo, Extensive reuse of soda-lime waste glass in fly ash-based geopolymers, Construct. Build. Mater. 188 (2018) 1077–1084.
[14] M.I. Cyr, Properties of inorganic polymer (geopolymer) mortars made of glass cullet, J. Mater. Sci. 47 (6) (2012) 2782–2797.
[15] A.G. Rincón, Novel 'inorganic gel casting' process for the manufacturing of glass foams, J. Eur. Ceram. Soc. 37 (5) (2017) 2227–2234.
[16] I.F.-J. Garcia-Lodeiro, Alkaline activation of synthetic aluminosilicate glass, Ceram. Int. 40 (4) (2014) 5547–5558.
[17] Y.C. Yang, pH-dependence of pesticide adsorption by wheat-residue-derived black carbon, Langmuir 20 (16) (2004) 6736–6741.
[18] N.V. Saha, Cationic dye adsorption on hydrochars of winery and citrus juice industries residues: performance, mechanism, and thermodynamics, Energies 13 (18) (2020) 4686.
[19] H.S. Aguiar, Structural study of sol–gel silicate glasses by IR and Raman spectroscopies, J. Non-Cryst. Solids 355 (8) (2009) 475–480.
[20] M.A. Longhi, New selective dissolution process to quantify reaction extent and product stability in metakaolin-based geopolymers, Compos. B Eng. 176 (2019), 107172.
[21] I.F.-J. García-Lodeiro, FTIR study of the sol–gel synthesis of cementitious gels: C–S–H and N–A–S–H, J. Sol. Gel Sci. Technol. 45 (1) (2008) 63–72.
[22] M. Hujova, P. M, New glass-based binders from engineered mixtures of inorganic waste, Int. J. Appl. Glass Sci. 12 (2021) 570–580.

[23] D.W. Green, Perry's Chemical Engineers' Handbook, McGraw-Hill Education, 2019.
[24] G.C. Tameni, Upcycling of boro-alumino-silicate pharmaceutical glass in sustainable construction materials, Detritus (20) (2022) 17.
[25] D.C. Lago, Adsorption of CsCl on porous SiO2 glass surface: experimental results and ab-initio calculations, J. Non-Cryst. Solids 440 (2016) 70–75.
[26] J.R. Rouquerol, Adsorption by Powders and Porous Solids: Principles, Methodology and Applications, Academic press, 2013.
[27] L.M.-C. Mihaly-Cozmuta, Adsorption of heavy metal cations by Na-clinoptilolite: equilibrium and selectivity studies, J. Environ. Manag. 137 (2014) 69–80.
[28] J.J. Gulicovski, Point of zero charge and isoelectric point of alumina, Mater. Manuf. Process. 23 (6) (2008) 615–619.
[29] P. Tian, Effect of pH on effective slip length and surface charge at solid–oil interfaces of roughness-induced surfaces, Micromachines 12 (7) (2021) 752.
[30] M.M. Šuránek, The study of Cu(II) adsorption onto synthetically modified geopolymers, Sustainability 15 (4) (2023) 2869.
[31] H.M.-B. Baykara, The use of zeolite-based geopolymers as adsorbent for copper removal from aqueous media, R. Soc. Open Sci. 9 (3) (2022), 211644.
[32] M.S.-M. Al-Harahsheh, Fly ash based geopolymer for heavy metal removal: a case study on copper removal, J. Environ. Chem. Eng. 3 (3) (2015) 1669–1677.
[33] A.S. Aziz, Kinetic modeling and isotherm studies for copper (II) adsorption onto palm oil boiler mill fly ash (POFA) as a natural low-cost adsorbent, Bioresources 9 (1) (2014) 336–356.
[34] E.D. Demirbas, Adsorption kinetics and equilibrium of copper from aqueous solutions using hazelnut shell activated carbon, Chem. Eng. J. 148 (2–3) (2009) 480–487.
[35] R.H. Devamani, Synthesis and characterisation of copper II hydroxide nano particles, Nano Biomed. Eng 5 (3) (2013) 116–120.
[36] R.L. Frost, Vibrational spectroscopy of selected minerals of the rosasite group, Spectrochim. Acta Mol. Biomol. Spectrosc. 66 (4–5) (2007) 1068–1074.
[37] C.T. Henrist, Study of the morphology of copper hydroxynitrate nanoplatelets obtained by controlled double jet precipitation and urea hydrolysis, J. Cryst. Growth 254 (1–2) (2003) 176–187.
[38] J.M. Aguirre, Simple route for the synthesis of copper hydroxy salts, J. Braz. Chem. Soc. 22 (2011) 546–551.
[39] S. Azizian, Kinetic models of sorption: a theoretical analysis, J. Colloid Interface Sci. 276 (1) (2004) 47–52.
[40] C.C. Addison, Volatile copper nitrate, an unusual coordination complex, J. Inorg. Nucl. Chem. 8 (1958) 569–571.
[41] M.O. Prado, On the sinterability of crystallizing glass powders, J. Non-Cryst. Solids 354 (40–41) (2008) 4589–4597.
[42] A. Ray, A. T, Compaction and sintering behaviour of glass–alumina composites, Mater. Chem. Phys. 67 (2001) 220–225.
[43] E. Bernardo, Sintering behaviour and mechanical properties of Al2O3 platelet-reinforced glass matrix composites obtained by powder technology, Ceram. Int. 30 (5) (2004) 785–791.
[44] I.V. Morozov, Thermal decomposition of Cu(NO3)2· 3H2O at reduced pressures, Thermochim. Acta 403 (2) (2003) 173–179.
[45] D.O. Russo, Sintered Glasses for High-Level Wastes, MRS Online Proceedings Library (OPL), 1996, p. 465.
[46] E.B. Bernardo, Optimisation of sintered glass–ceramics from an industrial waste glass, Ceram. Int. 36 (5) (2010) 1675–1680.
[47] M. Schneider, The cement industry on the way to a low-carbon future, Cement Concr. Res. 124 (2019), 105792.